Potential Enhancement in Atmospheric New Particle Formation by Amine-Assisted Nitric Acid Condensation at Room Temperature

Kuanfu Chen[1], Kai Zhang[1,2] and Chong Qiu[*,3]

Affiliations:

1 Division of Natural and Applied Sciences, Duke Kunshan University, Kunshan, Jiangsu 215300, China

2 Data Science Research Center (DSRC), Duke Kunshan University, Kunshan, Jiangsu 215300, China

3 Department of Chemistry and Chemical & Biomedical Engineering, University of New Haven, West Haven, Connecticut 06516, USA

Corresponding author: CHONG QIU (CQIU@newhaven.edu)

Abstract

Atmospheric aerosol plays a critical role in global climate and public health. Recent laboratory experiments showed that new particle formation is significantly enhanced by rapid condensation of nitric acid and ammonia at low temperatures. Amines are derivatives of ammonia with a significant presence in the atmosphere. For example, the wide implementation of amine-based Post-Combustion Carbon Capture (PCCC) units may significantly increase the ambient alkanolamine and polyamine levels. Using thermodynamic simulations, the condensation of alkylamines, alkanolamines and polyamines with nitric acid at various temperatures was systematically evaluated. Alkylamines will condense with nitric acid at temperatures comparable to that of ammonia. However, with additional hydrogen bonding groups, alkanolamines and polyamines may condense with nitric acid at room temperature, suggesting a new potential pathway to remove these amines from the atmosphere. Our results suggest the potentially critical role of amines in the atmospheric new particle formation via condensation with nitric acid to rapidly grow freshly nucleated clusters over their critical size at a higher temperature than ammonia. The condensed amines and nitric acid can also facilitate water uptake by aerosol particles at low relative humidity, which may alter their subsequent atmospheric transformations.

Highlights:

- Nitric acid can condense on nanoparticles with amines at a comparable or higher temperature than with ammonia
- Amines with additional hydrogen bonding ability can condense with nitric acid at room temperature
- Condensation of nitric acid and amines can grow freshly nucleated clusters significantly to facilitate new particle formation at various temperatures
- Condensation with nitric acid can be a significant removal pathway for amines, especially those with two or more hydrogen bonds
- Particles condensed with amines and nitric acid may absorb water at low relative humidity to influence their subsequent atmospheric aging

Graphics Abstract Art
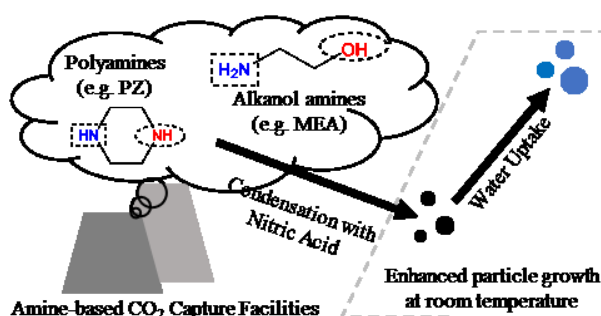
Keywords:
new particle formation, atmospheric cluster growth, room-temperature nitrate condensation, atmospheric amines, amine-based post-combustion carbon capture, aerosol hygroscopicity

1. Introduction

Amines are emitted into the atmosphere in large quantities from natural sources and anthropogenic activities (Qiu and Zhang, 2013; Cape et al., 2011; Ge et al., 2011a). Ambient amine concentrations are generally at a parts per trillion (ppt) level and at least 1–2 orders of magnitude lower than that of ammonia (Yli-Juuti et al., 2013); Methylamine (MA) and Dimethylamine (DMA) are two representative alkylamines commonly found in ambient gas and particle phases (Cape et al., 2011). A significant source of anthropogenic amines is chemical absorption Post-Combustion Carbon Capture (PCCC) technology using alkanolamines (e.g. monoethanolamine, MEA) and polyamines (e.g. piperazine, PZ) (Chao et al., 2021). While a large-scale application of amine-based PCCC units can effectively mitigate the raising ambient CO_2 level and the trends in climate change (Nielsen et al, 2012), such industrial application of amines will inevitably increase their emissions into the atmosphere (Reynolds et al, 2012). It is estimated that 80 tons of gaseous MEA will be emitted into the atmosphere by a PCCC unit removing one million tons of CO_2 annually (Sharma et al, 2014). In some extreme cases, the near-source ambient MEA concentrations can be comparable to that of ammonia (Scottish EPA, 2015) and reach to parts per million (ppm) level (Tian et al., 2022). Previous studies suggested several possible pathways for the removal of atmospheric amines, including gas-phase oxidation (Møller et al, 2020) that may lead to potentially hazardous products of nitramine and nitrosamine (Nielsen et al., 2011), new particle formation (NPF) and growth events involving sulfuric acid (SA) (Kürten et al., 2019; Yao et al., 2018; Almeida et al., 2013; Zhang et al., 2012), and heterogenous uptake by the acidic constituents in atmospheric aerosol (Tian et al., 2022; Qiu et al., 2011; Wang et al., 2010). Ammonia and amines related to this study are collectively referred as reduced nitrogen compounds (RNCs) and their properties are summarized in Table 1.

Nitric acid (NA), directly emitted from natural and anthropogenic sources and produced from gas-phase photochemical processes (Mezuman et al., 2016; Fairlie et al., 2010; Brown et al., 2006), has a significant presence in the atmosphere as high as 10^{12} cm^{-3} (Kumar et al., 2018b; Acker et al., 2005; Aloiso and Francisco et al., 1999) in some polluted areas (Ding et al., 2019; Zhang et al., 2018). Recent laboratory experiments reported rapid ammonia and nitric acid (NA) condensation on freshly nucleated clusters (FNCs) at or below 278 K (+5 °C) using ammonia, SA and NA concentrations comparable to those commonly found in the urban atmosphere, offering new insights into a ternary RNC, SA and NA nucleation system under cold weather conditions (Wang et al., 2020).

Since the nitrates of alkylamines and MEA showed better thermal stability than that of ammonium nitrate (Salo et al., 2011), it is conceivable that the cluster growth in a ternary amine-SA-NA system can be enhanced by amine and NA condensation. The reaction kinetics between several RNCs and NA were investigated in the gas phase (Chee et al., 2019; Kumar et al., 2018a) using the Density Function Theory (DFT) and Atmospheric Clusters Dynamic Code (ACDC) (Elm et al., 2020). Several pathways for the RNC and NA to co-condense and facilitate cluster growth were discovered and they are thermodynamically preferred at lower temperature (The formation equilibrium constants of 1:1 RNC-NA cluster at 270 K were 8-15 times higher than those at 298 K) and depend strongly on the RH of the system. Theoretical simulations on the condensation of RNCs and NA at the air-water interface (Kumar et al., 2018a) suggested an interesting contribution of the hydrogen bond between the RNC and water to facilitate the cluster formation at the interface. Liu et al. (2021) demonstrated that

adding the pathway of FNC growth due to DMA and NA co-condensation to the current simulation model can bring closure between theoretical prediction involving only the DMA-SA nucleation and field measurement results in polluted areas in the winter time (~280 K). Anthropogenic alkanolamines and polyamines from industrial processes, such as MEA and PZ widely used in PCCC, may, therefore, also be removed by gas-phase NA and contribute to the growth of FNCs and ambient nanoparticles, especially near their emission sources (such as PCCC units).
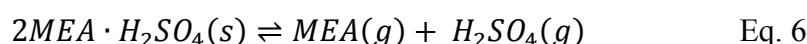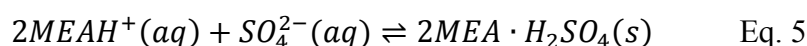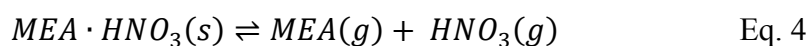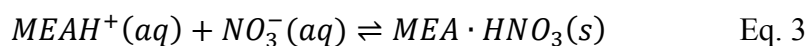
In this study, the condensation removal of amines with NA on nanoparticles was investigated using Extended Aerosol Inorganics Models (E-AIM) (Ge et al., 2011b; Wexler and Clegg, 2002) under conditions that are typically found in the atmosphere, especially in an urban environment. Our results showed that alkylamines can condense with NA at a comparable temperature (~273 K) to ammonia. Interestingly, significant condensation of MEA and PZ with NA was observed at room temperature (298 K), as well as other industrial alkanolamines that can form two or more hydrogen bonds. Such process seems to be unaffected by the presence of excess ammonia. Our results suggest that amines may be removed from the atmosphere by co-condensing with NA on nanoparticles in a wide range of temperatures. Such condensation may contribute to NPF by assisting the growth of FNCs into a critical diameter (of several nanometers) to avoid being scavenged by coagulation with other particles (Smith et al., 2020). Our results may be important in regions commonly polluted with amine emissions, such as megacities, agricultural lands and heavily industrialized areas.

2. Method
2.1 Overview.
The Extended-Aerosol Inorganics Model (E-AIM) considers the partitions of a particular chemical in four phases: gas (g), solid (s, including its salts), aqueous solution (aq) and hydrophobic organic solution (org) at any given relative humidity and temperature in a fixed total volume of 1 m^3 and at a fixed total pressure of 101,325 Pa. The E-AIM model (http://www.aim.env.uea.ac.uk/aim/aim.php) allows the users to specify the initial concentration of the chemical (as moles in 1 m^3), as well as instructions regarding the properties and activity of the chemical.

In this study, for example, the following series of state equations are possible for MEA (with its conjugated acid labeled as MEAH$^+$):

$$MEA\ (g) \rightleftharpoons MEA(aq) \qquad\qquad \text{Eq. 1}$$

$$MEA\ (aq) + H^+(aq) \rightleftharpoons MEAH^+(aq) \qquad\qquad \text{Eq. 2}$$

$$MEAH^+(aq) + NO_3^-(aq) \rightleftharpoons MEA \cdot HNO_3(s) \qquad\qquad \text{Eq. 3}$$

$$MEA \cdot HNO_3(s) \rightleftharpoons MEA(g) + HNO_3(g) \qquad\qquad \text{Eq. 4}$$

$$2MEAH^+(aq) + SO_4^{2-}(aq) \rightleftharpoons 2MEA \cdot H_2SO_4(s) \qquad\qquad \text{Eq. 5}$$

$$2MEA \cdot H_2SO_4(s) \rightleftharpoons MEA(g) + H_2SO_4(g) \qquad\qquad \text{Eq. 6}$$

Each of the equation above involves an equilibrium constant K that is temperature dependent and may have been determined experimentally or can be derived using other thermodynamic properties of MEA.

2.2 Application of E-AIM on RNC–SA–NA System.

    We used E-AIM to evaluate the equilibrium state of a chemical system involving SA, NA, ammonia and amines under varying temperatures (260 K to 330 K, or −13 °C to 57 °C), relative humidity (RH, 10% to 90%), and initial moles of the chemicals. The total pressure and volume were fixed at 101,325 Pa and 1 m^3, respectively. The typical initial moles of NA, SA and an RNC were 1.11151×10^{-9}, 2.03777×10^{-11} and 8.86895×10^{-8}, respectively, corresponding to a mixing ratio of 24 pptv NA, 0.44 pptv SA and 1915 pptv RNC at 60 % RH, 263.15 K, and 101,325 Pa. These values were chosen to represent typical atmospheric compositions in polluted megacities (Wang et al., 2020).

    All possible states for water (g, aq and s) are considered by the E-AIM. However, in this study, low temperatures at which the water may start to freeze were avoided. The autoprotolysis of water and both hydrolysis equilibria of the inorganic diacid H_2SO_4 are also considered to include H^+, HSO_4^- and OH^- concentrations in the calculations. The protonation of ammonia and the formation of ammonium nitrate and sulfate solids are considered in our simulations to represent the partition of ammonia in aqueous solution and solid phases as accurately as possible. Since NH_4^+, SO_4^{2-} and NO_3^- are the primarily inorganic ions of consideration, E-AIM Model II was used throughout our study. Thermodynamic data on ammonia and its nitrate and sulfate salts have been extensively studied and their thermodynamic properties and constants are relatively well established (Wexler and Clegg, 2002) Therefore, default inputs (including the methods to estimate activities) in the existing E-AIM Model II on ammonia, sulfuric acid and nitric acid are used without further modification. Detailed descriptions and justifications of the simulation parameters can be found in Section 4.1.

    Several chemicals in this study have multiple forms in condensed phases. For example, NA may exist in an aqueous solution as a free acid and a nitrate anion. Since the primary interest of this study is the distribution of a chemical in gas and condensed phases, the moles of all forms of a chemical in all condensed phases were aggregated together. For example, the total moles of NA as free acid and nitrate were reported together as the moles of condensed NA, $n_{cond.}(NO_3^-)$.

3. Results

    Our E-AIM simulation on ammonia and SA binary system showed the complete condensation of the sulfate into the solid phase as ammonium sulfate. In a ternary system of ammonia-SA-NA, ammonia and NA (Figure 1a) can condense into particle phase when the temperature is low enough (273 K and below). Wang et al. (2020) identified that ammonia and nitric acid in the ammonia-sulfuric acid-nitric acid ternary system could only condense at or below 278 K, but above 263 K, suggesting that our simulation results on the ammonia-SA-NA ternary system should have an uncertainty within the range of −3.8% to +1.7%.

    Our simulations used initial ammonia, SA and NA concentrations significantly exceeding the saturation vapor pressure of ammonium sulfate and nitrate (Wang et al., 2020; Liu et al., 2018; Ge et al., 2011b). As the temperature decreases, more and more condensed ammonia and NA will exist in condensed phase. This prediction is consistent with experimental findings that ammonia and NA in such ternary system could only condense at or below 278 K (Wang et al., 2020).
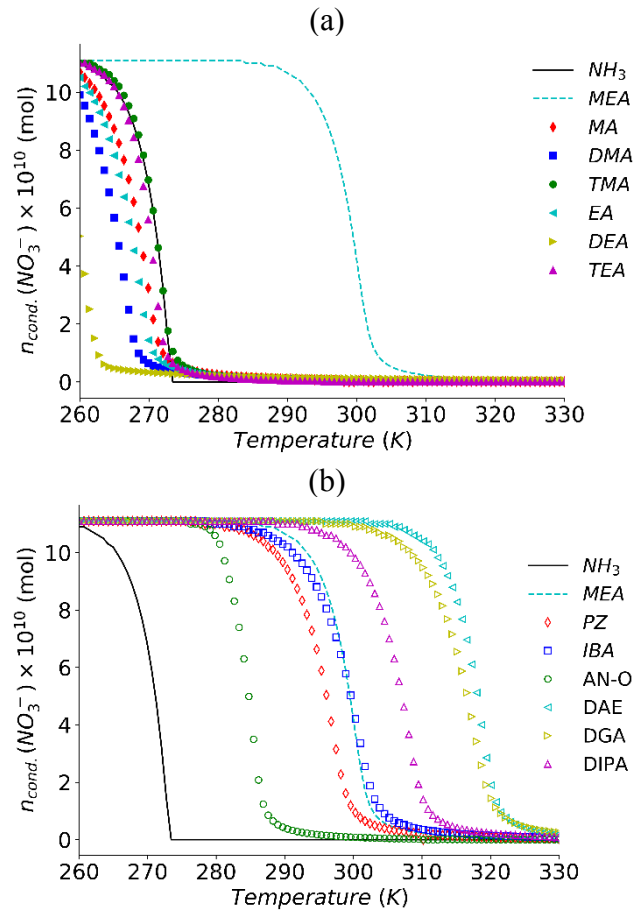
(a)

(b)

Figure 1. The moles of condensed nitrate against temperature in a ternary system of RNC-sulfuric acid-nitric acid at fixed initial water vapor of 0.07848 mol (equivalent to 60% RH at 263.15 K and 101325 Pa in 1 m³). All curves have the same initial moles of HNO_3, H_2SO_4 and the RNC as $1.11151×10^{-9}$, $2.03777×10^{-11}$ and $8.86895×10^{-8}$, respectively. The legend on the right indicates which RNC is present in each trace. (a) includes all RNCs in Group I (defined in Table 1) and MEA (as comparison) and (b) includes all RNCs in Group II and ammonia (as comparison).

Our simulations on a ternary system of alkylamine, SA and NA suggested that alkylamines such as MA and DMA condensed with NA at about 270 K, similar to that of ammonia (Figures 1a). The concentrations of alkylamines can be significant in urban and coastal environment from anthropogenic and biogenic emissions and may therefore contribute to NPF events in cold weather by facilitating the condensation of available gaseous NA on the FNCs.

Interestingly, alkanolamines such as MEA can condense with NA at room temperature (Figures 1b), suggesting its potential contribution to NPF under warmer weather conditions. Since ammonia is not likely to contribute to the NA condensation at room temperature (Wang et al., 2020; Liu et al., 2018), our findings suggest that gaseous MEA may contribute to NPF and be effectively removed by NA even in the presence of ammonia, especially at room temperature. Such observation is not limited to alkanolamines: PZ with two amine groups can also condense with NA at room temperature (Figure 1b).

In our simulations, the initial amines and NA concentrations should significantly exceed the saturation vapor pressures of aminium nitrate which are expected to be no

225   more than that of ammonium nitrate (Salo et al., 2011). It is also noted that in our
226   simulations the limiting reagents of the condensation process are the acids in the system.
227   The moles of condensed RNC did not exceed those of condensed sulfate (fixed in all
228   cases) and nitrate. Therefore, condensed nitrate directly reflects the amount of
229   condensed RNC in the particle phase. To quantitatively describe the condensation of
230   RNCs and nitrate, the transitional temperature of condensation (T_c), which is defined
231   as the temperature at which the moles of total nitrate in the condensed phases equal to
232   5% of the initial moles of NA, was identified and summarized in Table 1, along with
233   the estimated uncertainties. Our methods to estimate these uncertainties are presented
234   in Section 4.1, Figure 2 and Table 2.

236 **4. Discussion**
237 **4.1 Estimation of Uncertainties.**
238 **4.1.1 Effects of the Saturation Vapor Pressure of Amines.**
239   Data on the saturation vapor pressure (p^0) of an amine at various temperatures are
240   needed to accurately describe its distribution between gaseous and condensed phases.
241   However, comprehensive and high-quality experimental data on p^0 of amines are not
242   always available. Ge et al. (2011b) systematically evaluated the available experimental
243   data and several theoretical vapor pressure calculation models for amines and
244   concluded that the method by Moller et al. (2008) provides the best estimations.
245   Alkanolamines, such as MEA, showed the largest difference in calculated and measured
246   vapor pressure values (up to a factor of 3.56 times). Such discrepancy was much smaller
247   among monoamines with alkyl groups (a factor of 1.06). The default p^0 values for
248   amines in the E-AIM models were experimental data and only when these data were
249   missing, the calculation method by Moller et al. (2008) was used, with the exception of
250   MA, DMA, EA, DEA and AN-N (discussed in Section 4.1.2). In our study, to provide
251   the most conservative estimation of the uncertainties caused by errors in p^0 of amines,
252   the vapor pressure of each amine was increased and decreased by a factor of 3.56,
253   representing the maximum uncertainty range by the method of Moller et al. (2008),
254   while the rest of the conditions remained the same (initial moles of nitric acid, sulfuric
255   acid and an amine at 1.11151×10^{-9}, 2.03777×10^{-11} and 8.86895×10^{-8}, respectively,
256   initial mole of water at 0.07848 that corresponds to 60 % RH at 263.15 K and 101,325
257   Pa). Figure 2(a) illustrates the results of such error analysis using PZ as an example.
258   The corresponding T_c values are summarized in Table 2 and the relative uncertainties
259   were generally small (± 3%).

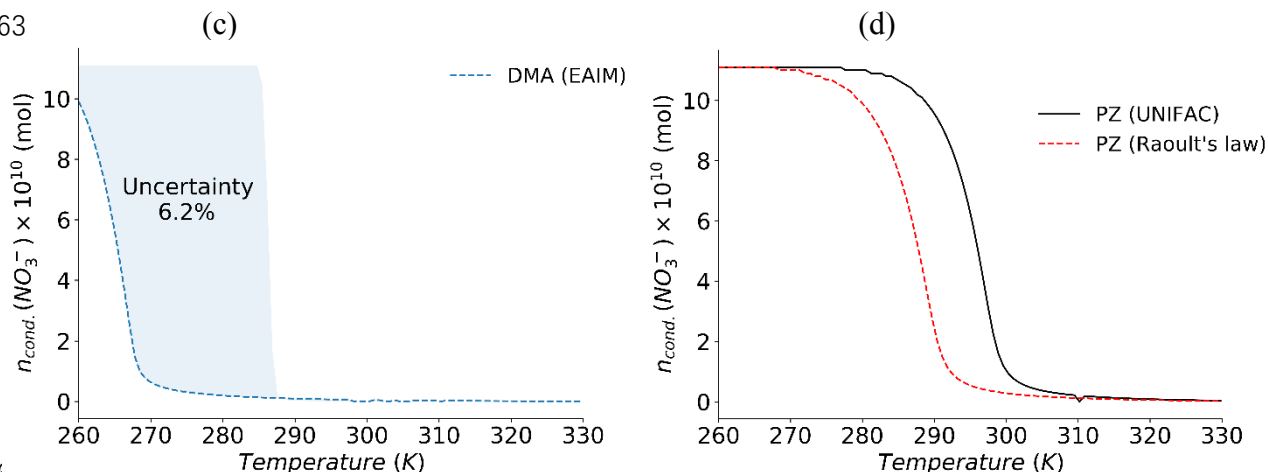261   (a)   (b)

262
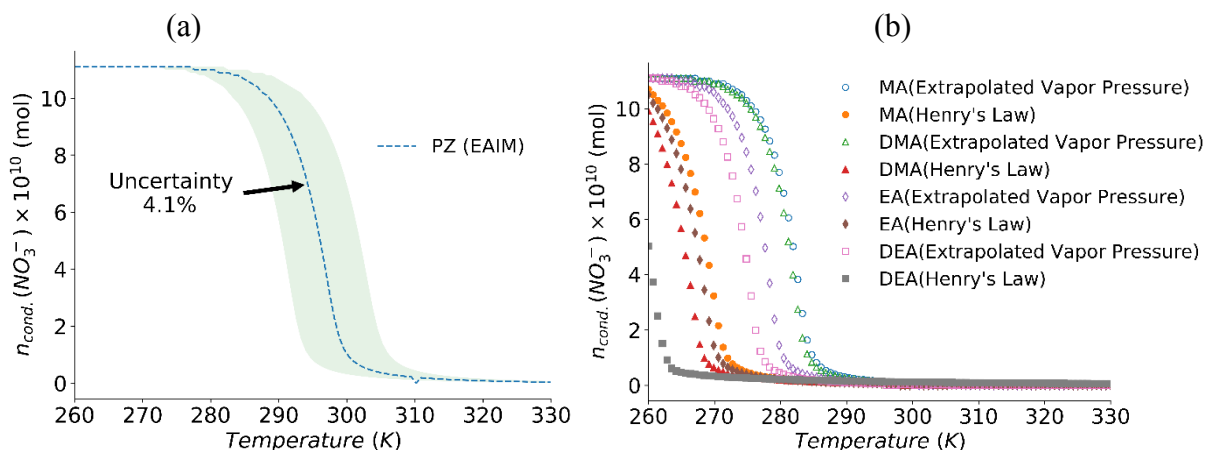
Figure 2. (a) The uncertainties in T_c of PZ (gray area) resulting from the uncertainties in its saturation vapor pressure p^0. The dash line represents the results using p^0 values recommended by Ge et al (2011b). The lower and upper boundaries of the gray area were derived by increasing and decreasing the vapor pressure by a factor of 3.56, respectively. (b) The differences in T_c for MA, DMA, EA and DEA when using Henry's law constant K_H (hallow markers) and the extrapolated vapor pressure p^0 at 298 K (solid markers). The extrapolated vapor pressures were based on their Antoine Equations at low temperatures (Linstrom and Mallard, 2018). (c) The uncertainties in T_c of DMA (gray area) resulting from the uncertainties in its Henry's law constant K_H at 298 K. The dash line represents the results using the K_H at 298 K value recommended by Linstrom and Mallard (2018). The lower and upper boundaries of the gray area were derived by using the minimum and maximum K_H at 298 K values (with clearly stated methods of determination) in Sander (2015), respectively. (d) The comparison in T_c values of PZ using different activity estimation methods. The black solid line was calculated with the UNIFAC method and the red dash line was based on Raoult's law.

To evaluate the Kelvin curvature effect (Zhang et al., 2012) on the condensation of RNC and NA, the saturation vapor pressure p_{sat} of MEA was increased by factors of 10 (9 nm particle diameter) and 10^2 (4.5 nm particle diameter). This p_{sat} range was estimated based on the 0.050 J m^{-2} surface free energy value for the nitrates of MEA (Greaves et al. 2006) and a calculated molar volume of 259 mol cm^{-3} (Salo et al. 2011). The corresponding T_c values decreased to 296 K and 288 K, respectively. This analysis suggests the significant impact of particle size on the condensation of RNCs and NA. However, a systematic evaluation of uncertainties from the Kelvin effect was not conducted due to the limited available information on the physical properties of the nitrate salts of amines.

4.1.2 Effects of the Henry's Law constant of monoamines

MA, DMA, EA and DEA are monoamines with small alkyl group(s) and their measured p^0 ranges (described by the Antoine equation parameters) are generally well below 298 K (Linstrom and Mallard, 2018). Opposite to these small alkylamines, AN-N has extremely low p^0 at 298 K and therefore has an Antoine equation applicable only at 415–609 K (Linstrom and Mallard, 2018). It is therefore difficult to use p^0 to study these amines, without introducing unknown levels of uncertainties by extrapolating their Antonie equations to 298 K. Alternatively, Henry's Law constant K_H for these amines can be used to describe their partition between gas and aqueous solution and has been determined on these amines previously (Linstrom and Mallard, 2018; Sander, 2015). The values recommended by Ge et al. (2011b) were considered the default input

302 parameters in our study (corresponding results reported in Table 1).

303   Additional simulations were carried out using the extrapolated p^0 for each of the
304 five monoamines with initial moles of the nitric acid, sulfuric acid and amine at
305 1.11151×10^{-9}, 2.03777×10^{-11} and 8.86895×10^{-8}, respectively, and a fixed initial mole
306 of water at 0.07848 (corresponding to 60 % RH at 263.15 K and 101,325 Pa). The
307 results were plotted in Figure 2(b), except for AN-N which showed negligible
308 difference (< 0.05%). While the results for the four alkylamines using the K_H and the
309 extrapolated p^0 appeared to be very different, it is important to note that in all four cases
310 the T_c values calculated using the extrapolated p^0 values are higher than those calculated
311 using the K_H values, suggesting that the reported T_c values in our Table 2 are the lower
312 bound estimation of the transitional temperature at which the amines can condense with
313 nitric acid. Numerically, the choice to use K_H or extrapolated p^0 for our simulations will
314 cause a change in T_c values by 6% or less.

315   Due to the potentially large errors in extrapolating the p^0 values, the variability in
316 the T_c of DMA associated with its extrapolated p^0 was further tested by increasing and
317 decreasing its extrapolated p^0 at 298 K by a factor of 4.8 (limited by the maximum
318 allowed p^0 value of 10 atm in E-AIM). In the case of AN-N, the extrapolated p^0 value
319 at 298 K from Antoine equation was lower by 30 times based on another vapor pressure
320 estimation method, EPI Suite v 4.11 (US EPA, 2019). The corresponding relative
321 uncertainties in T_c caused by these drastic changes in extrapolated p^0 values were within
322 2%.

323   It is also important to note the complications in applying the K_H values from
324 literatures in our thermodynamic simulations. The K_H values at 298 K for the five
325 amines vary significantly in literatures (Sander, 2015). In our simulations, the K_H values
326 recommended by Linstrom and Mallard (2018) were used as default input values
327 (corresponding results reported in Table S1). When applicable, the largest and smallest
328 K_H values of an amine (with clearly stated method of determination) at 298 K
329 summarized by Sander (2015) were used to estimate the possible uncertainties caused
330 by the variability in K_H at 298 K. Figure 2(c) illustrated such uncertainty estimation on
331 DMA as an example. The T_c values after varying the K_H values at 298 K for the four
332 amines are included in Table 2.

333   Note that among available data, there are also significant uncertainties in the
334 temperature dependence of K_H for amines. A systematic uncertainty analysis was
335 difficult due to the lack of such literature data for most of the amines in our study, which
336 could be a potential issue in the accurate determination of T_c values. However, for the
337 five amines with available alternative temperature dependence coefficients of K_H
338 (Sander, 2015), the uncertainties in T_c values caused by the alternative coefficients are
339 within 3%.

340

341 **4.1.3 Effects of the Activity of amines**

342   It is possible to carry out thermodynamic simulations with or without considering
343 the activities of the chemicals in the aqueous solution, including the ammonium and
344 aminium cations, the nitrate and sulfate anions and the dissolved amines. The scenario
345 where activities of all chemical species are considered to be one is referred as the
346 Raoult's law method, which is likely applicable at high relative humidity due to the
347 much-diluted ion concentrations. However, at a higher temperature or lower relative
348 humidity, water condensation on the particle may be limited and the formed aqueous
349 solution may have a very high ionic strength (Pye et. al., 2020). Therefore, it is

important to evaluate the uncertainties caused by the methods used for activity estimations in our simulations.

The activities of the anions involved in our simulations were relatively well studied (Wexler and Ge, 2002). Ge et al. (2011b) showed that it is reasonable to assume the activities of the aminium cations to be the same as that of ammonium cation. As highly polar molecules, the activities of amines dissolved in an aqueous solution may be described using the UNIFAC method (Fredenslund, 1977).

Our T_c values reported in Table 1 were based on simulations using the UNIFAC method as default to estimate the activities of the amines. Ge et al. (2011b) showed that the estimation of activities of amines using UNIFAC method will generally lead to satisfactory results yet the dataset for comparison was far from comprehensive. Therefore, additional simulations were carried out using the Raoult's law method for all the amines. One example comparing the results between Raoult's law and UNIFAC methods is shown in Figure 2(d). The relative difference in T_c using the two activity estimation methods for amines in our study was generally below 2.5%.

4.1.4 Effects of the Solubility of the Nitrate Salts of Amines

One last potential complication in our thermodynamic simulations is the possible formation of the solid aminium nitrate salts. Only a handful of the nitrates of alkylamines (such as MA, DMA, TMA), AN and MEA were studied for their solubility properties. The general trend is that the nitrate salts of alkylamines and alcohol amines are highly soluble in water, which consequentially makes no impact on the thermodynamic modeling results.

In the case of AN, its nitrate salt has low solubility. Additional simulation using E-AIM while specifying the solubility of AN nitrate showed that no solid of AN nitrate may form under our simulation conditions. It is therefore reasonable to assume that the water solubility of the aminium nitrate salts had no impact on our T_c results.

4.1.5 Overall uncertainty estimations

As discussed previously, it is assumed that the overall uncertainties of our simulation were determined by errors in p^0 (or K_H) estimations and the discrepancies in the activity estimation methods (assuming that the true value lies in the middle of the two methods), and the two sources were independent from each other. The uncertainties in the temperature dependence of K_H were not considered in our error estimations due to the large variability in the data in the literature. Instead, the values suggested by Linstrom and Mallard (2018) were used as the default values for the temperature dependence of K_H.

The overall uncertainty for the T_c value of each amine was therefore the square root of the square sum of the two independent sources (summarized in Table 2).

4.2 Temperature Dependence of Amine and Nitric Acid Co-condensation.

Our simulation results strongly suggest that amines can co-condense with nitric acid onto FNCs and nanoparticles in the atmosphere and the process depends on the temperature. For example, alkylamines commonly found in the atmosphere all showed T_c values ranging from 263 K to 275 K, similar to that of ammonia and implying the limited contribution of alkyl groups in the condensation of alkylamines with NA. Group I RNCs is hereby defined as those that will only condense with NA at or below 278 K. Other RNCs with T_c values at or above 288 K are collectively referred as Group II RNCs in this study. Our results indicate that NA-assisted condensation may serve as a

399 potentially significant removal process for Group II RNCs (e.g., MEA and PZ),
400 especially in warmer weather. Group II amines in the atmosphere may also greatly
401 facilitate the NPF by condensing with NA at room temperature to grow the critical
402 clusters over the "valley of death" with excessive particle savaging.
403   It is worth noting that typically the uncertainty of the upper boundary for the T_c
404 value is larger than that of the lower boundary. This is particularly pronounced in DEA
405 and may bring its T_c value up to the 280 K range. While the uncertainty analysis
406 presented in Table 2 could move some of the amines from Group I to Group II, it doesn't
407 change our conclusion that amines may contribute significantly to nitric acid
408 condensations in the presence of high ammonia concentration, especially at higher
409 temperature where ammonia and nitric acid are not likely to condense.
410
411 **4.3 Structural Dependence of Amine and Nitric Acid Co-condensation.**
412   To further elucidate the reason for the variance in T_c of the amines in the two groups.
413 the properties of amines with distinctively different functional groups (Table 1) were
414 compared to identify possible factors contributing to the significant difference in T_c
415 values among amines.
416   Neither gaseous basicity (GB), aqueous basicity (K_b) or the volatility of an RNC
417 (K_p) seems to directly determine the T_c of an RNC. For example, DMA and MEA have
418 similar GB values yet distinctively different T_c. When compared with PZ, TMA has a
419 similar K_b yet a T_c that is ~ 28 K lower. PZ has a much higher GB than MEA but their
420 T_c values are comparable. AN and MEA have similar saturation vapor pressures at room
421 temperature yet distinctive different T_c, ruling out any direct contribution on T_c from
422 the volatility of the amine.
423   To our surprises, the solid/gas dissociation constants of the nitrates of alkylamines
424 are about 10 times lower than that of ammonium nitrate yet they exhibit comparable T_c,
425 suggesting that saturation condensation of nitrate salts alone may not explain the
426 difference in T_c for Group I and II RNCs. As discussed later in Section 4.5, water
427 condensation was frequently observed even at low RH in our simulations involving
428 amines and NA. Previous studies have suggested a strong stabilization effect of particle
429 water content on the condensed aminium nitrates (Chee et al., 2019; Kumar et al.,
430 2018a).
431   Furthermore, the molar mass of IBA is about 50% more than that of MEA, but their
432 T_c values are essentially the same, suggesting that Van der Waals forces do not
433 contribute significantly here. It appears that the electron affinity of the functional
434 groups on the amines has little effect on the T_c. For example, the nitro group in AN-N
435 and the methyl group in AN-M are electron withdrawing and electron donating groups,
436 respectively. However, both RNCs showed little contribution to NA condensation at
437 above 260 K.
438   One distinctive observation is that amines with only alkyl (e.g., MA) or aromatic
439 (e.g., AN) substitutions showed much lower T_c than those with hydroxyl (–OH) groups
440 (e.g., MEA). Furthermore, IBA and PZ, showed T_c values comparable to that of MEA,
441 with the former having a similar chemical structure as MEA, while the latter having a
442 second amine group (–NH–) in the ring (Table 1). Since MEA and PZ do not share the
443 same functional groups, their high T_c values could not be explained alone by the
444 presence of –OH groups in the chemical structure.
445   It is therefore deducted that additional hydrogen bonding can significantly increase
446 the temperature at which an RNC may condense with NA, since Group I RNCs can
447 form only one hydrogen bond while Group II RNCs can form two or more (Table 1).

For example, MEA and PZ can form two hydrogen bonds and have T_c values of ~ 300 K. Alkanolamines that can form three hydrogen bonds, commonly used as industrial chemicals, showed T_c values as high as 323 K (Table 1), allowing condensation with NA above room temperature.

Another factor that may affect the T_c is hydrophobic functional groups of RNCs as there was a noticeable decrease in T_c value from MA to AN and AN-M. AN and AN-M both contain an aromatic ring which is more hydrophobic than a methyl group. As suggested by other theoretical analysis (Chee et al., 2019; Kumar et al., 2018a), it is hypothesized that any hydrophobic functional group of an RNC may hinder the formation of hydrogen bond between the nitrate of the RNC and water, resulting in less nitrate condensation. For example, in the case of AN-O, the –OH attached to the aromatic ring can form one additional hydrogen bond, which seems to offset the negative effect of the non-polar aromatic ring and increase the T_c to 289K (+15 °C).

4.4 Effects of Excess Ammonia on Amine and Nitric Acid Co-condensation.

Although Figure 1 well demonstrated the condensation of amines and NA in a wide range of temperatures, ambient amine concentrations vary significantly with the constant presence of ammonia. The ambient concentration of amines is usually 1–2 orders of magnitude lower than that of ammonia, but the amine:ammonia mol ratio could be as high as 1:1 near a power-plant using PCCC technology. As a result, a chemical system of ammonia, MEA, SA and NA with varying MEA:ammonia mol ratios was investigated. Figure 3(a) illustrated the additional condensation of nitrate as a result of added MEA.
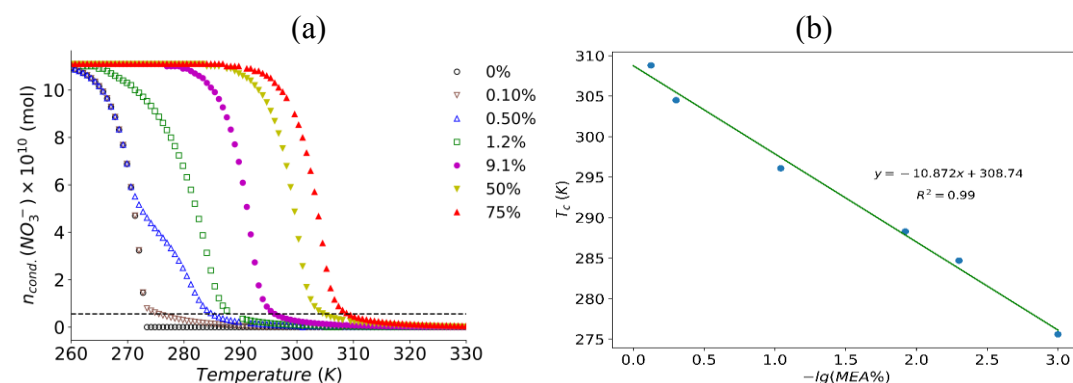

Figure 3. (a) The moles of condensed nitrate against temperature in an ammonia-MEA-sulfuric acid-nitric acid chemical system with varying mole ratios of ammonia and MEA. The legend indicates the initial mole fraction (mol %) of the MEA in the total moles of RNCs in each trace. (b) Linear relationships between the transitional temperature of nitric acid condensation (T_c, defined as the temperature at which the moles of total nitrate in the condensed phases equals to 5% of the initial moles of nitric acid and determined in this study.) and logarithm of MEA mole fraction (mol %) in total moles of RNCs (ammonia and MEA) in the system at 298K. All simulations have the same total moles of ammonia as 8.86895×10^{-8} and the same initial moles of HNO_3 and H_2SO_4 as 1.11151×10^{-9} and 2.03777×10^{-11}, respectively. The system has a fixed initial moles of water vapor as 0.07848 (equivalent to 60% RH at 263.15 K and 101,325 Pa in 1 m^3).

The enhancement in NA condensation was noticeable with as low as 0.1 mol % added MEA (~ 2 pptv). It appeared that as the mole fraction of MEA increases, the T_c increases following an excellent linear relationship (Figure 3b):

$$T_c = -10.872 \times log(MEA\%) + 308.74 \quad \text{Eq. 7}$$

where MEA% is the MEA mole fraction (mol %) in the total moles of all RNCs.

4.5 RH Dependence of Amine and Nitric Acid Co-condensation.

In addition to the structures and concentrations of amines, amount of total water is another factor that may impact the condensation of amines and NA. The condensation of DMA and NA was enhanced by the presence of water in a recent DMA-NA nucleation study (Chee et al., 2019). Our further investigation suggested that an increase in the total water vapor in the RNC-SA-NA system led to an increase in T_c, hence facilitating the condensation of amine and NA at a higher temperature (Figure 4a). However, the enhancement was not as strong as additional hydrogen bonding.

(a)

(b)
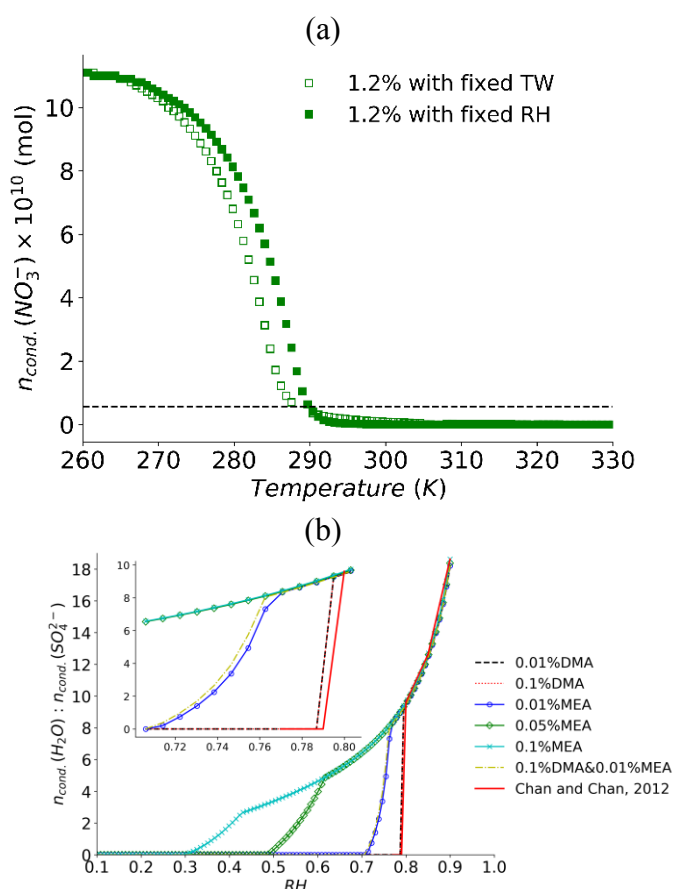
Figure 4. (a) The moles of condensed nitric acid against temperature with 1.2 mol % of MEA in total RNCs at fixed total water (TW) or fixed relative humidity (RH) in a chemical system of ammonia, MEA, sulfuric acid and nitric acid. Both curves have the initial moles of ammonia and MEA as 8.86895×10^{-8} and 1.06427×10^{-9}, respectively. The percentage refers to the mol % of MEA in moles of all RNCs (ammonia and MEA) in the system. For open square curve, the initial TW of the system was fixed at 0.07848 mol (equivalent to 60% RH at 263.15 K and 101,325 Pa in 1 m³). For solid square curve, the initial RH of the system was fixed at 60%. The black line is the T_c threshold. When the initial RH of the system was fixed in each simulation, as the temperature increased, the corresponding TW of the system also increased. (b) Hygroscopicity of a chemical system of RNCs-sulfuric acid-nitric acid at 298 K. The y-axis is the mole ratio of water and sulfate in the condensed phases. Difference traces represent the varying initial amine:ammonia mole ratios. All curves have the same total moles of RNCs as 8.86895×10^{-8}. The reference curve (red solid line based on Ref. Chan and Chan, 2012) only has ammonium sulfate. The legend indicates the initial mole fraction (mol %) of the amine(s)

519 in the total RNCs in each trace. Both panels have the same initial moles of HNO_3 and H_2SO_4
520 as 1.11151×10^{-9} and 2.03777×10^{-11}, respectively.
521
4.6 Hygroscopicity of Aerosol after Amine and Nitric Acid Co-condensation.

523   In addition to T_c, the onset RH at which aerosol starts to uptake water vapor may
524 also play an important role in the formation and growth of nanoparticles. While
525 ammonium nitrate may uptake water vapor at low RH, the condensation of ammonia
526 and NA is likely hindered at room temperature (Wang, 2020). Therefore, an ammonia-
527 SA-NA system without amines is expected to start absorbing water vapor at about 79%
528 RH like ammonium sulfate (Chan and Chan, 2012). The onset RH of water uptake by
529 the condensed phases at 298 K was systematically evaluated in an ammonia-SA-NA
530 system with additional DMA and MEA (representing Group I and II RNCs, respectively)
531 and varying amine:ammonia mole ratios (Figure 4b). In all cases, all the sulfate
532 condensed as ammonium sulfate; therefore, the mol ratio of condensed water to sulfate
533 is directly proportional to the moles of condensed water. Water update at 65% RH by a
534 mixture of ammonium nitrate-ammonium sulfate (Lee et al., 2008) was not observed in
535 our simulations, probably because of the anticipated lack of condensation of ammonium
536 nitrate at 298 K (Figure 1).
537   Adding 0.01 or 0.1 mol % of DMA (in the total moles of all RNCs) to the system
538 only promoted water update at a slightly lower RH (~78.5%). In contrast, MEA played
539 a significant role in lowering the onset RH of water uptake by the condensed phases.
540 For example, the presence of 0.01 and 0.1 mol % of MEA lowered the onset RH to ~71 %
541 and 30 %, respectively (Figure 4b), facilitating the water uptake by the condensed
542 phases in a dry environment. These observations are consistent with the hygroscopic
543 behavior of aminium (especially MEA) cations in aqueous solutions (Tian et al., 2022;
544 Rovelli et al., 2017; Chu et al., 2015; Clegg et al., 2013; Qiu and Zhang, 2012). The
545 system with 0.01 mol % MEA and 0.1 mol % DMA showed somewhat enhanced water
546 uptake by the condensed phases than the cases with only MEA or DMA (Figure 4b,
547 insert); however, the effect was limited and the presence of MEA was the main
548 contributor to the lowered onset RH. It seems that the enhancement of particle
549 hygroscopicity in an RNCs-SA-NA system is additive of the contributions from the
550 RNCs in the system and dominated by Group II RNCs.
551
4.7. Atmospheric Implications

553   Thermodynamic models are useful to evaluate how anthropogenic amines such as
554 MEA and PZ may condense with NA on atmospheric particles since the feasibility of
555 such process in the atmosphere is governed by the final physical and chemical equilibria
556 of the system. Our simulations suggest that there are two distinct groups of amines
557 (Table 1): Group I with a T_c of +5 °C or below and Group II with a T_c of +15 °C or
558 above. Both groups may assist condensation of NA on nanoparticles under various
559 ambient conditions and contribute to NPF in addition to their assistance in forming
560 FNCs (Yao et al., 2018; Almeida et al., 2013; Zhang et al., 2012), especially in polluted
561 urban, agricultural and industrial areas. However, since the growth of FNCs is largely
562 governed by the kinetics of the system, a careful evaluation of the reaction kinetics of
563 amine-nitric acid condensation is warranted.
564   The reaction rate constant of ammonia-NA condensation can be estimated based
565 on the lab experiments (Wang et al., 2020), which showed that ammonia and NA can
566 condense on clusters (with core diameters of 5–10 nm and primarily consisted of
567 ammonium sulfate) at a rate of ~ 45 nm per hour. In 45 minutes, the clusters grew into

nanoparticles with diameters of 39–44 nm and a number concentration of ~ 10^5 cm^{-3}. Assuming the net increase in particle size was solely from the condensation of ammonium nitrate with a material density of 1.72 g cm^{-3}, we estimated that the condensation flux of ammonium nitrate on nanoparticles was 1.4–2.1 × 10^7 cm^{-3} s^{-1}. Since the experiments were conducted with 1915 pptv ammonia and 24 pptv NA at 1 atm and 278 K, the concentrations of ammonia and NA were estimated to be 5 × 10^{10} and 6 × 10^8 cm^{-3}, respectively. The observed condensation rate of ammonia and nitrate at 278 K is therefore estimated as 4.5–6.5 × 10^{-13} cm^3 s^{-1}.

Several kinetic studies involving DFT and ACDC showed that DMA and NA condense at a faster rate (Liu et al., 2021; Chee et al., 2019; Kumar et al., 2018a) than that of ammonia and NA (Liu et al., 2018) on FNCs in the RNC-NA or RNC-NA-SA nucleation systems. It is reasonable to assume that alkanolamines such as MEA will condense with NA at a rate no slower than that of DMA. This assumption is based on the observation that MEA and PZ may form clusters with SA at a kinetic rate that is comparable or faster than that of DMA (Ma et al., 2019; Xie et al., 2017), suggesting that the condensation of MEA or PZ with NA will probably proceed no slower than that between DMA and NA. Such deduction is further supported by the substantially lower saturation vapor pressure of MEA nitrate compared to that of ammonium nitrate.

Since the nitrate of MEA has a molar mass of 124.10 and material density of 1.26 g cm^{-3} (Salo, 2011), its molar volume is estimated to be twice as that of ammonium nitrate. Assuming the same condensation rate of ammonia and NA, a ppm level of ambient MEA near a PCCC unit may lead to particle growth due to the MEA and NA (of 24 pptv) condensation at a rate as high as 57.8 nm per hour. Therefore, atmospheric clusters and nanoparticles may experience a significant growth near a PCCC unit due to MEA and NA condensation at room temperature. However, the particle growth will be significantly slower as moving away from the emission source of MEA.

Our estimations suggest a potentially significant removal pathway of Group II amines by condensation with NA in the atmosphere at room temperature regardless of ambient ammonia concentration and offer an alternative explanation to some field observations of unexpectedly abundant MEA in ambient nanoparticles (Huang et al., 2016; Zhang and Anastasio, 2003). Typically, at 278 K, MEA will react with hydroxyl radicals · OH (with a typical ambient concentration of c_{OH} = 10^6 cm^{-3}) at a rate of k_{OH} = 8 × 10^{-11} cm^3 s^{-1} (Xie et al., 2014). If MEA will condense with NA at a rate of k_{NA} = 5 × 10^{-13} cm^3 s^{-1} at 278 K as estimated above and the ambient concentration of NA is c_{NA} = 10^8 – 10^{10} cm^{-3}, the relative contribution of NA to the condensation removal of MEA in the atmosphere can be estimated as: $k_{NA} \cdot c_{NA}/(k_{OH} \cdot c_{OH})$ = 0.6 – 60, suggesting that the contribution of NA assisted condensation removal of MEA in the atmosphere can be as significant as gas-phase oxidations. Since most amines in Group II are anthropogenic alkanolamines (MEA) and polyamines (PZ), our results offer an additional pathway to consider when evaluating the ambient lifetime of industrial amines, especially under warmer weather conditions. This could be particularly important in areas with PCCC units using MEA or PZ. Our results also indicated that it is possible to aggregate the quantities of all Group II amines into a single mole fraction parameter to identify their maximum condensation temperature with NA for field and modeling applications.

Furthermore, our results suggest that even at very low concentrations, the condensed MEA and NA may facilitate the water uptake by aerosol to form a thin layer of solution at the particle surface (Hsiao et al., 2016). Such modification to the particle surface may change critical properties of aerosol, including the viscosity (Shiraiwa et

al., 2010), surface tension (Ovadnevaite et al., 2017) and Kelvin curvature effect (Zhang et al., 2012), redox reactivities (Kong et al., 2021), surface uptake and heterogeneous reactions (Rossignol et al., 2016; Kolb et al., 2011), hygroscopicity (Tian et al., 2022; Qiu and Zhang, 2012) and CCN potentials (Lavi et al., 2013).

5. Conclusions

Systematic thermodynamic simulations were conducted to evaluate the potential contribution of the condensation of atmospheric amines and nitric acid on the growth of atmospheric clusters and nanoparticles under various temperature and relative humidity conditions. Our results indicated two distinctly different groups of amines: Group I amines (e.g., MA and DMA) can only form one hydrogen bond and can condense with nitric acid under cold weather conditions, similar to ammonia; Group II amines (e.g. MEA and PZ) can form two or more hydrogen bonds and may condense with nitric acid near room temperature, independent of the ambient ammonia concentration. The condensed amines and nitric acid are likely to promote particle water uptake from the gas phase, which may facilitate further atmospheric transformation of the aerosol. Our findings also suggested an alternative removal pathway for atmospheric amines, especially those from industrial processes (e.g. PCCC technology).

Data Availability

E-AIM models are openly available at http://www.aim.env.uea.ac.uk/aim/aim.php. The original data used for the table and figures in the study are available at Harvard Dataverse via: https://doi.org/10.7910/DVN/WZJBHU with CC0 license.

References

Acker, K., Möller, D., Auel, R., Wieprecht, W. and Kalaß, D. Concentrations of nitrous acid, nitric acid, nitrite and nitrate in the gas and aerosol phase at a site in the emission zone during ESCOMPTE 2001 experiment. *Atmospheric Research*. **2005**, 74, 507–524.

Almeida, J., Schobesberger, S., Kürten, A., Ortega, I. K., Kupiainen-Määttä, O., et al. Molecular understanding of sulphuric acid-amine particle nucleation in the atmosphere. *Nature*. **2013**, 502, 359–363.

Aloisio, S. and Francisco, J. S. Structure and Energetics of Hydrogen Bonded HOx−HNO3 Complexes. *The Journal of Physical Chemistry A*. **1999**, 103, 6049–6053.

Brown, S. S., Ryerson, T. B., Wollny, A. G., Brock, C. A., Peltier, R., Sullivan, A. P., et al. Variability in nocturnal nitrogen oxide processing and its role in regional air quality. *Science*. **2006**, 311, 67–70.

Cape, J. N., Cornell, S. E., Jickells, T. D. and Nemitz, E. Organic nitrogen in the atmosphere — Where does it come from? A review of sources and methods. *Atmoshperic Research*. **2011**, 102, 30–48.

Chan, L. P. and Chan, C. K. Displacement of Ammonium from Aerosol Particles by Uptake of Triethylamine. *Aerosol Science and Technology*. **2012**, 46(2), 236-247.

Chao, C., Deng, Y., Dewil, R. Baeyens, J. and Fan, X. Post-Combustion Carbon Capture. *Renewable Sustainable Energy Rev*. **2021**, 138, 110490.

Chee, S., Myllys, N., Barsanti, K. C., Wong, B. M. and Smith, J. N. An Experimental and Modeling Study of Nanoparticle Formation and Growth from Dimethylamine and Nitric Acid. *The Journal of Physical Chemistry A*. **2019**, 123, 5640–5648.

Chu, Y., Sauerweina, M. and Chan, C. K. Hygroscopic and phase transition properties of alkyl aminium sulfates at low relative humidities. *Physical Chemistry Chemical Physics*. **2015**, 17, 19789-19796.

Clegg, S., Qiu, C. and Zhang, R., The deliquescence behaviour, solubilities, and densities of aqueous solutions of five methyl- and ethyl-aminium sulphate salts, *Atmospheric Environment*. **2013**, 73, 145–158.

Ding, J., Zhao, P., Su, J., Dong, Q., Du, X. and Zhang, Y. Aerosol pH and its driving factors in Beijing. *Atmospheric Chemistry and Physics*. **2019**, 19, 7939–7954.

Elm, J., Kubečka, J., Besel, V., Jääskeläinen, M. J., Halonen, R., Kurtén, T. and Vehkamäki, H. Modeling the formation and growth of atmospheric molecular clusters: A review. *Journal of Aerosol Science*. **2020**, 149, 105621.

Fairlie, T. D., Jacob, D. J., Dibb, J. E., Alexander, B., Avery, M. A., van Donkelaar, A. and Zhang, L. Impact of mineral dust on nitrate, sulfate, and ozone in transpacific Asian pollution plumes. *Atmospheric Chemistry and Physics*. **2010**, 10, 3999–4012.

698

699 Fredenslund, A., Gmehling, J., Michelson, M. L., Rasmussen, P. and Prausnitz, J. M.
700 Computerized Design of Multicomponent Distillation Columns Using the UNIFAC
701 Group Contribution Method for Calculation of Activity Coefficients. *Industrial &*
702 *Engineering Chemistry, Process Design and Development*. **1977**, 16, 450–462.

703

704 Ge, X., Wexler, A. S. and Clegg, S. L. Atmospheric amines — Part I. A review.
705 *Atmospheric Environment*. **2011a**, 45, 524–546.

706

707 Ge, X., Wexler, A. S. and Clegg, S. L. Atmospheric amines — Part II. Thermodynamic
708 properties and gas/particle partitioning. *Atmospheric Environment*. **2011b**, 45, 561–577.

709

710 Greaves, T. L., Weerawardena, A., Fong, C., Krodkiewska, I. and Drummond, C. J.
711 Protic Ionic Liquids: Solvents with Tunable Phase Behavior and Physicochemical
712 Properties. *The Journal of Physical Chemistry B*. **2006**, 110, 22479–22487.

713

714 Hsiao, T. C., Young, L. Y, Tai, Y. C. and Chen, K. C. Aqueous film formation on
715 irregularly shaped inorganic nanoparticles before deliquescence, as revealed by a
716 hygroscopic differential mobility analyzer-aerosol particle mass system. *Aerosol*
717 *Science and Technology*. **2016**, 50, 568–577. DOI: 10.1080/02786826.2016.1168512
718

719 Huang, X., Deng, C., Zhuang, G., Lin, J. and Xiao, M. Quantitative Analysis of
720 Aliphatic Amines in Urban Aerosols Based on Online Derivatization and High
721 Performance Liquid Chromatography. *Environmental Science: Processes & Impacts*.
722 **2016**, 18 (7), 796−801.

723

724 Hunter, E. P. L. and Lias, S. G. Evaluated Gas Phase Basicities and Proton Affinities of
725 Molecules. *Journal of Physical and Chemical Reference Data*. **1998**, 27, 413–656.

726

727 Kolb, C. E., Williams, L. R., Jayne, J. T. and Worsnop, D. R. Mass accommodation and
728 chemical reactions at gas-liquid interfaces. *Chemical Reviews*. **2011**, 111, 76–109.

729

730 Kong, X., Castarède, D., Thomson, E. S., Boucly, A., Artiglia, L., Ammann, M.,
731 Gladich, I. and Pettersson, J. B. C. A surface-promoted redox reaction occurs
732 spontaneously on solvating inorganic aerosol surfaces. Science. **2021**, 374, 747–752.

733

734 Kumar, M., Li, H., Zhang, X., Zeng, X. C. and Francisco, J. S. Nitric Acid–Amine
735 Chemistry in the Gas Phase and at the Air–Water Interface. *Journal of the American*
736 *Chemical Society*. **2018a**, 140, 6456-6466.

737

738 Kumar, M., Zhong, J., Zeng, X. C. and Francisco, J. S. Reaction of Criegee Intermediate
739 with Nitric Acid at the Air–Water Interface. *Journal of the American Chemical Society*.
740 **2018b**, 140, 4913–4921.

741

742 Kürten, A. New particle formation from sulfuric acid and ammonia: nucleation and
743 growth model based on thermodynamics derived from CLOUD measurements for a
744 wide range of conditions. *Atmospheric Chemistry and Physics*, **2019**, 19, 5033-5050.
745 DOI: 10.5194/acp-19-5033-2019.

746

Lavi, A., Bluvshtein, N., Segre, E., Segev, L., Flores, M., et al. Thermochemical, cloud condensation nucleation ability, and optical properties of alkyl aminium sulfate aerosols. *The Journal of Physical Chemistry A*. **2013**, 117, 22412–22421.

Lee, A. K. Y., Linga T. Y. and Chan C. K. Understanding hygroscopic growth and phase transformation of aerosols using single particle Raman spectroscopy in an electrodynamic balance. *Faraday Discuss*. **2008**, 137, 245-263

Linstrom, P. J. and Mallard, W. G. (eds.). *NIST Chemistry WebBook, NIST Standard Reference Database Number 69*. **2018**, National Institute of Standards and Technology, Gaithersburg (MD), http://webbook.nist.gov (retrieved August, 2021).

Liu, L., Li, H., Zhang, H., Zhong, J., Bai, Y., et al. The role of nitric acid in atmospheric new particle formation. *Physical Chemistry Chemical Physics*. **2018**, 20, 17406–17414.

Liu, L., Yu, F., Du, L., Yang, Z., Francisco, J. S. and Zhang, X. Rapid sulfuric acid-dimethylamine nucleation enhanced by nitric acid in polluted regions. *Proceedings of the National Academy of Sciences of the United States of America*. **2021**, 118(35). DOI: 10.1073/pnas.2108384118

Ma, F., Xie, H.-B., Elm, J., Shen, J., Chen, J., Vehkamäki, H., et al. Piperazine Enhancing Sulfuric Acid-Based New Particle Formation: Implications for the Atmospheric Fate of Piperazine. *Environmental Science & Technology*. **2019**, 53, 8785–8795.

Mezuman, K., Bauer, S. E. and Tsigaridis, K. Evaluating secondary inorganic aerosols in three dimensions. *Atmospheric Chemistry and Physics*. **2016**, 16, 10651–10669.

Moller, B., Rarey, J. and Ramjugernath, D. Estimation of the vapor pressure of non-electrolyte organic compounds via group contributions and group interactions. *Journal of Molecular Liquids*. **2008**, 143, 53–63.

Møller, K. H., Berndt T. and Kjaergaard, H. G. Atmospheric Autoxidation of Amines. *Environmental Science & Technology*. **2020**, 54 (18), 11087–11099.

Nielsen, C. J., D'Anna, B., Dye, C., Graus, M., Karl, M., et al. Atmospheric Chemistry of 2-Aminoethanol (MEA). *Energy Procedia*. **2011**, 4, 2245−2252.

Nielsen, C. J., Herrmann, H. and Weller, C. Atmospheric chemistry and environmental impact of the use of amine in carbon capture and storage (CCS). *Chemical Society Reviews*. **2012**, 41, 6684–6704.

Ovadnevaite, J., Zuend, A., Laaksonen, A., Sanchez, K. J. and Roberts, G. Surface tension prevails over solute effect in organic-influenced cloud droplet activation. *Nature*. **2017**, *544*, 637–641.

Pye, H. O. T., Nenes, A., Alexander, B., Ault, A. P., Barth, M. C., Clegg, S. L., et al. The acidity of atmospheric particles and clouds. *Atmospheric Chemistry and Physics*. **2020**, 20, 4809–4888.

Qiu, C., Wang, L. Lal, V., Khalizov, A. F. and Zhang, R. Heterogeneous Reactions of Alkylamines with Ammonium Sulfate and Ammonium Bisulfate. *Environmental Science & Technology*. **2011**, 45, 11, 4748-4755.

Qiu, C. and Zhang, R. Physicochemical properties of alkylaminium sulfate: Hygroscopicity, thermostability and density. *Environmental Science & Technology*. **2012**, *46*, 4474–4480. DOI: 10.1021/es3004377

Qiu, C. and Zhang, R. Multiphase chemistry of atmospheric amines. *Physical Chemistry Chemical Physics*. **2013**, 15, 5738–5752.

Reynolds, A. J., Verheyen, T. V., Adeloju, S. B., Meuleman, E. and Feron, P. Towards Commercial Scale Postcombustion Capture of CO_2 with Monoethanolamine Solvent: Key Considerations for Solvent Management and Environmental Impacts. *Environmental Science & Technology.* **2012**, 46 (7), 3643−3654.

Rossignol, S., Tinel, L., Bianco, A., Passananti, M., Brigante, M., et al. Atmospheric photochemistry at a fatty acid-coated air-water interface. *Science*. **2016**, 353, 699–702.

Rovelli, G., Miles, R. E. H., Reid, J. P. and Clegg, S. L. Hygroscopic properties of aminium sulfate aerosols. *Atmospheric Chemistry and Physics*. **2017**, 17, 4369–4385.

Salo, K., Westerlund, J., Andersson, P. U., Nielsen, C. and D'Anna, B. et al. Thermal characterization of aminium nitrate nanoparticles. *The Journal of Physical Chemistry A*. **2011**, 115, 11671−11677.

Sander, R. Compilation of Henry's law constants (version 4.0) for water as solvent. *Atmospheric Chemistry and Physics*. **2015**, 15, 4399–4981.

Scottish Environment Protection Agency (Scottish EPA). Review of amine emissions from carbon capture systems, v2.01. **2015**, Retrieved from https://www.sepa.org.uk/media/155585/review-of-amine-emissions-from-carbon-capture-systems.pdf

Sharma, S. D. and Azzi, M. A. Critical Review of Existing Strategies for Emission Control in the Monoethanolamine-Based Carbon Capture Process and Some Recommendations for Improved Strategies. *Fuel.* **2014**, 121, 178−188.

Shiraiwa, M., Ammann, M., Koop, T. and Pöschl, U. Gas uptake and chemical aging of semisolid organic aerosol particles. *Proceedings of the National Academy of Sciences of the United States of America*. **2010**, 108, 11,003–11,008.

Smith, J. N., Danielle, C. D., Sabrina, C., Michelia, D., Hayley, G., et al. Atmospheric clusters to nanoparticles: Recent progress and challenges in closing the gap in chemical composition. *Journal of Aerosol Science*. **2020**, 153, 105733.

Tian, X., Chu, Y. and Chan, C. K. Reactive Uptake of Monoethanolamine by Sulfuric Acid Particles and Hygroscopicity of Monoethanolaminium Salts. *Environmental Science & Technology Letters*. **2022**, 9, 16−21

845

846 United States Environmental Protection Agency (US EPA). **2019**, Estimation Programs
847 Interface Suite™ for Microsoft® Windows, v 4.11. (retrieved September, 2021).
848

849 Wang, L., Khalizov, A. F., Zheng, J., Xu, W., Ma, Y., et al. Atmospheric nanoparticles
850 formed from heterogeneous reactions of organics. *Nature Geoscience.* **2010**, 3, 238–
851 242.
852

853 Wang, M., Kong, W., Marten, R., He, X.-C., Chen, D., et al. Rapid growth of new
854 atmospheric particles by nitric acid and ammonia condensation. *Nature.* **2020**, 581,
855 184–189.
856

857 Wexler, A. S. and Clegg, S. L. Atmospheric aerosol models for systems including the
858 ions H^+, NH_4^+, Na^+, SO_4^{2-}, NO_3^-, Cl^-, Br^- and H_2O. *Journal of Geophysical Research.*
859 **2002**, 107, D14.
860

861 Xie, H.-B., Li, C., He, N., Wang, C., Zhang, S. and Chen, J. Atmospheric Chemical
862 Reactions of Monoethanolamine Initiated by OH Radical: Mechanistic and Kinetic
863 Study. *Environmental Science & Technology.* **2014**, 48 (3), 1700−1706.
864

865 Xie, H.-B., Elm, J., Halonen, R., Myllys, N., Kurtén, T., Kumala, M., et al.
866 Atmospheric Fate of Monoethanolamine: Enhancing New Particle Formation of
867 Sulfuric Acid as an Important Removal Process. *Environmental Science & Technology.*
868 **2017**, 51, 8422–8431.
869

870 Yao, L., Garmash, O., Bianchi, F., Zheng, J., Yan, C., et al. Atmospheric new particle
871 formation from sulfuric acid and amines in a Chinese megacity. *Science.* **2018**, 361,
872 278–281.
873

874 Yli-Juuti, T., Barsanti, K., Hildebrandt Ruiz, L., Kieloaho, A.-J., Makkonen, U., Petäjä,
875 T., et al. Model for acid-base chemistry in nanoparticle growth (MABNAG).
876 *Atmospheric Chemistry and Physics.* **2013**, 13, 12,507–12,524.
877

878 Zhang, Q. and Anastasio, C. Free and Combined Amino Compounds in Atmospheric
879 Fine Particles (PM2.5) and Fog Waters from Northern California. *Atmospheric
880 Environment.* **2003**, 37, 2247.
881

882 Zhang, R. Y., Khalizov, A., Wang, L., Hu, M. and Xu, W. Nucleation and growth of
883 nanoparticles in the atmosphere. *Chemical Reviews.* **2012**, 112, 1957–2011.
884

885 Zhang, R., Sun, X., Shi, A., Huang, Y., Yan, J., Nie, T., Yan, X. and Li, X. Secondary
886 inorganic aerosols formation during haze episodes at an urban site in Beijing, China.
887 *Atmospheric Environment.* **2018**, 177, 275–282.
888

Table 1. The chemical structures and properties of reduced nitrogen compounds (RNCs) involved in this study.
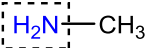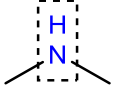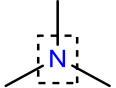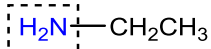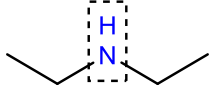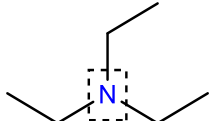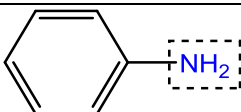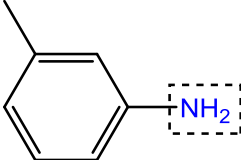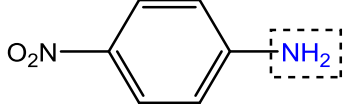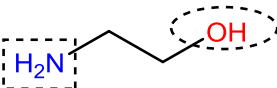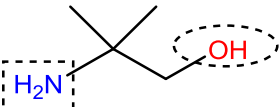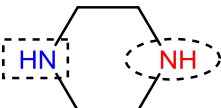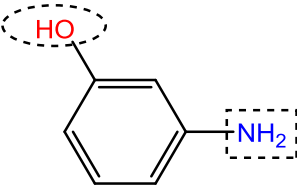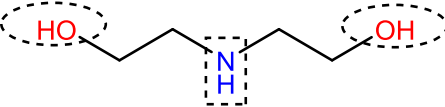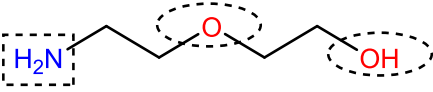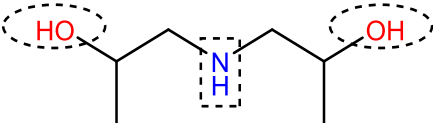
RNC name	Abbreviation	Chemical Structure	p_{sat} [a]	GB [b]	K_b [c]	K_p [d]	T_c [e]	Group [f]
Ammonia	NH$_3$	NH$_3$	9.94×10^5	819.0	1.76×10^{-5}	4.48×10^{-7}	$273.4^{+4.6}_{-10}$	I
Methylamine	MA	H$_2$N—CH$_3$	9.75×10^{4} †	864.5	4.57×10^{-4}	4.54×10^{-8}	$274.1^{+15}_{-3.6}$	I
Dimethylamine	DMA		5.37×10^{4} †	896.5	5.38×10^{-4}	6.27×10^{-8}	$270.6^{+17}_{-3.0}$	I
Trimethylamine	TMA		2.31×10^5	918.1	6.33×10^{-5}	1.65×10^{-6}	$274.8^{+5.8}_{-5.5}$	I
Ethylamine	EA	H$_2$N—CH$_2$CH$_3$	1.39×10^{5} ‡	878.0	4.46×10^{-4}	2.83×10^{-8}	$272.7^{+15}_{-0.8}$	I
Diethylamine	DEA		3.00×10^{4} ‡	919.4	6.90×10^{-4}	7.01×10^{-9}	$263.9^{+24}_{-7.7}$	I
Triethylamine	TEA		9.03×10^3	951	5.62×10^{-4}	$9.39 \times 10^{-8*}$	273.8^{+10}_{-10}	I
Aniline	AN		8.52×10^1	850.6	7.41×10^{-10}	1.01×10^{-4}	$256.6^{+2.8}_{-2.8}$	I
3-Methylaniline	AN-M		1.07×10^1	864.0	5.13×10^{-10}	-	$256.6^{+4.4}_{-4.4}$	I
p-Nitroaniline	AN-N		6.79×10^{-2} ‡	834.2	1.05×10^{-13}	-	$256.6^{+0.1}_{-0.1}$	I
Monoethanol amine	MEA		6.51×10^1	896.8	3.16×10^{-5}	$1.41 \times 10^{-12*}$	$304.5^{+5.2}_{-4.9}$	II

Name	Abbrev.	Structure	a	b	c	d	e	f
Isobutanol amine	IBA		7.48×10^1	-	7.25×10^{-5}	-	$307.0^{+7.1}_{-7.1}$	II
Piperazine	PZ		5.32×10^2	914.7	5.38×10^{-5}	-	$302.4^{+4.8}_{-5.1}$	II
3-Aminophenol	AN-O		3.80×10^{-3}	866.9	2.34×10^{-10}	-	$289.0^{+4.6}_{-4.9}$	II
Diethanol amine	DAE		6.87×10^{-2}	920	9.77×10^{-6}	$9.14 \times 10^{-13*}$	$323.5^{+4.9}_{-4.9}$	II
Diglycol amine	DGA		1.54×10^{-1}	-	5.01×10^{-6}	-	$323.7^{+6.8}_{-6.5}$	II
Diisopropanol amine	DIPA		5.67×10^{-1}	-	9.12×10^{-6}	-	$313.5^{+6.6}_{-6.6}$	II

[a] The saturation vapor pressure (in Pa) of the amine at 298 K (Ge et al., 2011b; Linstrom and Mallard, 2018).

[b] The gaseous basicity (in kJ·mol^{-1}) at 298 K (Hunter and Lias, 1998).

[c] The aqueous base hydrolysis constant (in mol·kg^{-1}) of the amine at 298.15 K (Ge et al., 2011b).

[d] The solid/gas equilibrium dissociation constant (in Pa^2) of the nitrate salt of the amine at 298.15 K (Ge et al., 2011b).

[e] The transitional temperature (in K) of nitric acid condensation, defined as the temperature at which the moles of total nitrate in the condensed phases equals to 5% of the initial moles of nitric acid and determined in this study. Details on uncertainty estimations are in Table 2.

[f] classified based on the T_c of the amine: Group I amines with $T_c \leq 278$ K and Group II with $T_c > 288$ K.

[†] At 266 K; [‡] Extrapolated to 298 K based on the Antoine Equation (Linstrom and Mallard, 2018); [*] At 293 K.

Table 2. Uncertainty estimations of the T_c values for the reduced- nitrogen compounds (RNCs) in this study.

RNC	T_c [a]	Upper limit of T_c due to p^0 (298 K) [b]	Lower limit of T_c due to p^0 (298 K) [b]	Difference in T_c due to activity [c]	Overall uncertainty in T_c, upper limit [d]	Overall uncertainty in T_c, lower limit [d]
NH$_3$	273.4	-	-	-	+ 1.7%[**]	− 3.8%[**]
MA	274.1	288.4[*]	274.1[*]	-2.5%[†]	+ 5.4%	− 1.3%
DMA	270.6	287.3[*]	270.6[*]	-2.2%[†]	+ 6.3%	− 1.1%
TMA	274.8	279.6	270.6	-2.4%	+ 2.1%	− 2.0%
EA	272.7	288.0[*]	272.0[*]	-0.2%[†]	+ 5.6%	− 0.3%
DEA	263.9	287.4[*]	257.9[*]	3.5%[†]	+ 9.1%	− 2.9%
TEA	273.8	278.4	269.7	6.7%	+ 3.8%	− 3.7%
AN	256.6	256.6	256.6	2.2%	+ 1.1%	− 1.1%
AN-M	256.6	256.6	256.6	3.6%	+ 1.7%	− 1.7%
AN-N	256.6	256.5[*]	256.7[*]	< 0.05%[‡]	<+0.05%[#]	<− 0.05%[#]
MEA	304.5	309.6	299.9	-0.9%	+ 1.7%	− 1.6%
IBA	307.0	314.0	300.0	-1.1%	+ 2.3%	− 2.3%
PZ	302.4	308.8	296.5	-2.5%	+ 2.5%	− 2.3%
AN-O	289.0	293.0	284.7	1.7%	+ 1.6%	− 1.7%
DAE	323.5	328.5	318.6	-0.2%	+ 1.5%	− 1.5%
DGA	323.7	330.6	317.3	0.1%	+ 2.1%	− 2.0%
DIPA	313.5	319.5	307.5	1.9%	+ 2.1%	− 2.1%

The transitional temperature (in K) of nitric acid condensation assisted with the amine by using default E-AIM input parameters.
[b] The limits of the T_c (in K) resulting from the uncertainties in vapor pressure p^0 at 298 K of the amine (unless noted otherwise). The upper and lower limits of T_c were obtained by decreasing and increasing p^0 at 298 K of the amine by a factor of 3.56, respectively.
[c] The relative difference in T_c between the UNIFAC and the Raoult's law methods to determine activities of the amine in an aqueous solution.
[d] It is assumed that the uncertainty in T_c was caused mainly by the uncertainties of the p^0 (or K_H when applicable) and activity estimations.
[†] This uncertainty was within ± 0.05% when the Henry's law constant K_H of the amine was used. It was then conservatively estimated by using the extrapolated vapor pressure at 298 K based on the Antoine Equation of the amine.[5] The enthalpy change at 298 K was extrapolated based on

compiled data by Linstrom and Mallard (2018). The heat capacity was assumed to be the same as that of TMA, -90 J•mol^{-1}•K^{-1}.

‡ Both enthalpy change values of 70.0 kJ/mol and 77.9 kJ/mol[5] produced similar results (<0.05% difference).

* The limits of the T_c (in K) resulting from the uncertainties in the Henry's law constant K_H at 298 K. The upper and lower limits of T_c were obtained by choosing the maximum and minimum K_H values at 298 K from available literature values with stated method of determination in Sander (2015). The temperature dependence of the Henry's law constants was based on the values recommended by Linstrom and Mallard (2018).

** The relative uncertainties were estimated by comparing with the experimental observations (263 – 278 K) by Wang et al (2020).

$^\#$ The relative uncertainties were less than 0.05%.